Cerebral Cortex September 2007;17:2204–2213
doi:10.1093/cercor/bhl127
Advance Access publication November 23, 2006

Morphological, Electrophysiological, and Synaptic Properties of Corticocallosal Pyramidal Cells in the Neonatal Rat Neocortex

Jean-Vincent Le Bé[1], Gilad Silberberg[1,2], Yun Wang[3] and Henry Markram[1]

[1]Laboratory of Neural Microcircuitry, Brain Mind Institute, Ecole Polytechnique Fédérale de Lausanne (EPFL), Lausanne 1015, Switzerland, [2]Nobel Institute for Neurophysiology, Department of Neuroscience, Karolinska Institute, Stockholm, Sweden and [3]Division of Neurology Research, Caritas St Elizabeth's Medical Center, Tufts University, Boston, MA, USA

Neocortical pyramidal cells (PCs) project to various cortical and subcortical targets. In layer V, the population of thick tufted PCs (TTCs) projects to subcortical targets such as the tectum, brainstem, and spinal cord. Another population of layer V PCs projects via the corpus callosum to the contralateral neocortical hemisphere mediating information transfer between the hemispheres. This subpopulation (corticocallosally projecting cells [CCPs]) has been previously described in terms of their morphological properties, but less is known about their electrophysiological properties, and their synaptic connectivity is unknown. We studied the morphological, electrophysiological, and synaptic properties of CCPs by retrograde labeling with fluorescent microbeads in P13–P16 Wistar rats. CCPs were characterized by shorter, untufted apical dendrites, which reached only up to layers II/III, confirming previous reports. Synaptic connections between CCPs were different from those observed between TTCs, both in probability of occurrence and dynamic properties. We found that the CCP network is about 4 times less interconnected than the TTC network and the probability of release is 24% smaller, resulting in a more linear synaptic transmission. The study shows that layer V pyramidal neurons projecting to different targets form subnetworks with specialized connectivity profiles, in addition to the specialized morphological and electrophysiological intrinsic properties.

Keywords: corpus callosum, neocortex, pyramidal neurons, synaptic connections

Introduction

Transfer of information between the 2 neocortical hemispheres is essential for a variety of cognitive processes, such as perception, memory, attention, and learning (Engel et al. 1991; Matsuzaka et al. 1999; Eliassen et al. 2000; Aboitiz et al. 2003; Quigley et al. 2003). Information is directly transferred between the 2 neocortical hemispheres by axons of a specialized subpopulation of neocortical pyramidal cells (PCs) via the corpus callosum. Neocortical PCs exhibit a large diversity, which is mainly evident in their different morphological properties (Simons and Woolsey 1984; Hirsch et al. 1998) and projection targets (Katz 1987; Hubener and Bolz 1988; Kasper et al. 1994; Zhang and Deschenes 1997; Thomson and Bannister 2003). Layer V PCs project to various targets, including subcortical nuclei (White and Hersch 1982; Cho et al. 2004), cortical regions in the same hemisphere (Zhang and Deschenes 1998), and the contralateral hemisphere (Katz 1987; Hubener and Bolz 1988). The differences in the morphological properties of the different PC subpopulations (Hubener and Bolz 1988; Tsiola et al. 2003; Vercelli et al. 2004; Yuste 2005) suggest that they integrate cortical activity differently, thus conveying different aspects of the cortical activity to the various efferent targets. The electrophysiological and synaptic properties of the different PC subpopulations are also likely to affect their respective functions.

Corticocallosally projecting cells (CCPs) project to the contralateral hemisphere via the corpus callosum. They are characterized by a small soma and a short apical dendrite that does not display a tuft in layer I, strikingly different from the extensively studied layer V thick tufted PCs (TTCs) that have a big soma and a thick apical dendrite forming tuft dendrites in layer I and project their axons to the tectum, brainstem, and the spinal cord (Hubener and Bolz 1988; Kasper et al. 1994). Previous reports showed electrophysiological (Kasper et al. 1994; Christophe et al. 2005) and genetic (Christophe et al. 2005) differences between the TTCs and the CCPs. A systematic study of the CCPs synaptic properties is however still lacking. In this study, CCPs were selectively labeled by retrograde injection of fluorescent microbeads to the contralateral hemisphere and then recorded by multineuron whole-cell recordings followed by 3-dimensional morphological reconstruction for detailed characterization. We describe here the morphological, electrophysiological, and synaptic properties of corticocallosal PCs in layer V of the rat somatosensory neocortex.

Materials and Methods

Injections

CCPs labeling was done by injections of fluorescent microbeads (Lumafluor, Naples, FL, 4× diluted in nano-pure water) into the left hemisphere of P11 (postnatal 11 days) Wistar rats (Fig. 1*A*). These beads are retrotransported by the axons that terminate at the site of injection. The rats were anesthetized with an intraperitoneal injection of Fentanyl–Medetomidine (mixed from Fentanyl IV solution at 0.05 mg mL^{-1} and Domitor solution at 1 mg mL^{-1} and completed with saline solution to get a 10 mL kg^{-1} injection and 0.3 mg kg^{-1} for both products). They were then fixed on a stereotaxic table (Stoelting Co., Wood Dale, IL) and their head skin opened with a scalpel sagittally from between the eyes to between the ears. The skin was then gently pushed aside, and the skull cleaned with a dry cotton piece. The smooth skull was then pierced at the injection sites with a Neolus 25G × 5/8″ syringe needle (Terumo Europe N.V., Leuven, Belgium). It was then cleaned again, and the beads were injected with a Hamilton syringe inserted 1 mm below the skull surface. A volume of 0.5 μL per site was injected in 3 sites 1 mm lateral and 0 ± 1 mm from Bregma in the left hemisphere (somatosensory cortex, S1). In order to get a good diffusion at the injection site, the syringe was retracted 60 s after the end of the injection. The wound was then glued with chirurgical glue (Histoacryl, Braun Aesculap, Tuttlingen, Germany) and the rats awakened with Atipamezole–Naloxone (1 mg kg^{-1} and 0.1 mg kg^{-1}, respectively, mixed from Antisedan solution at 5 mg mL^{-1} and Narcan solution at 0.4 mg mL^{-1} and completed with saline to get a 10 mL kg^{-1} injection). After complete awakening (~20 min), the rats were returned to their mother's cage. All animal experimentations were performed under the Swiss guidelines for animal experiments.

Slicing

Three days following the injection of beads, the rats were rapidly decapitated, and sagittal slices (300 μm thick) of the right hemisphere

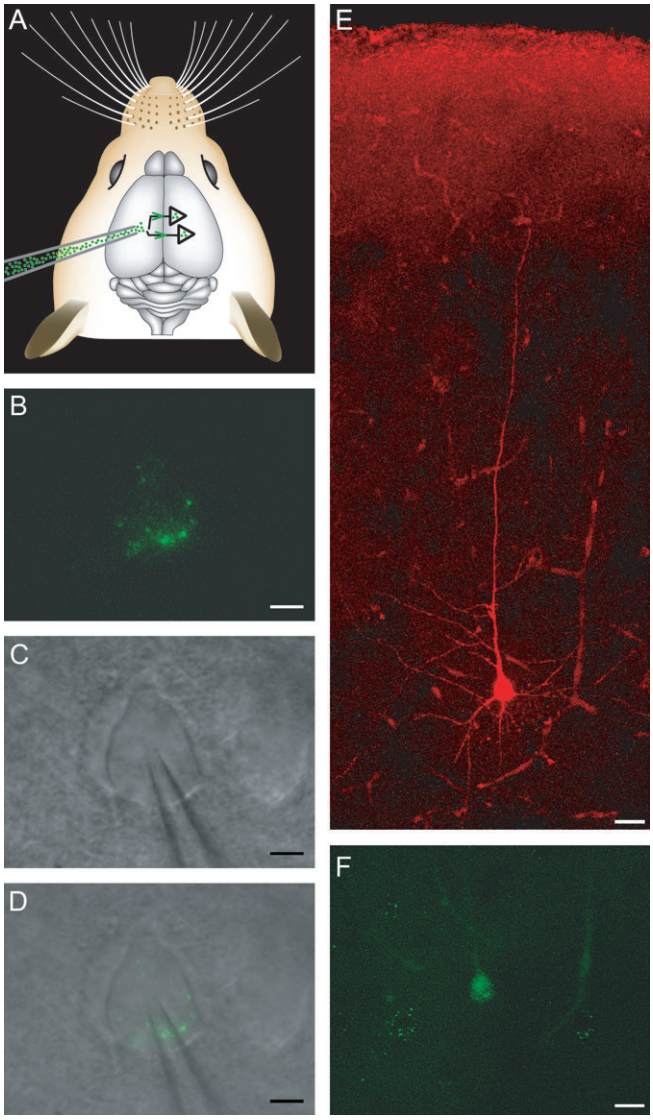

Figure 1. Isolation of the corticocallosally projecting PCs. (*A*) Schematics of the beads injection procedure. The beads are injected in layer V of the left hemisphere cortex. They then undergo retrograde transport (green arrows) to the right hemisphere (used for recordings) marking the cells projecting via the corpus callosum. (*B*) High-magnification picture of a retrograde-labeled pyramidal neuron. The green dots are the ~0.2-μm beads. Scale bar 5 μm. (*C*) The same view as in (*B*) but under IR-DIC imaging, showing the cell and the patch pipette. (*D*) Merge of (*B*) and (*C*). (*E*) Low-magnification fluorescence view of the cell in (*B*), (*C*), (*D*) filled with alexa red by the patch pipette. Scale bar 20 μm. (*F*) Low magnification of the region containing the cell mentioned (in plain green due to overlap with alexa red spectrum in the green region). Other cells marked with beads are present in the area showing the possibility to obtain paired recordings of the identified population. Scale bar 20 μm.

were cut in artificial cerebrospinal fluid (ACSF) on a slicer HR2 (Sigmann Elektronik, Heidelberg, Germany). The hemisphere was glued at the surface of the sagittal plane onto a block, which was mounted at an angle of 10° such that the blade cut from the upper part of the cortex toward the caudal border and down toward the midline. Slices were incubated for 15–30 min at 35 °C and then left at room temperature (20–22 °C). The ACSF contained (in mM) 125 NaCl, 2.5 KCl, 25 D-glucose, 25 $NaHCO_3$, 1.25 NaH_2PO_4, 2 $CaCl_2$, and 1 $MgCl_2$.

Fluorescence and infrared differential interference contrast (IR-DIC) Microscopy

Neurons in somatosensory cortex were identified using IR-DIC microscopy (Fig. 1*C*), with an upright microscope (BX 51WI, Olympus, fitted with a 60× LUMPlan FI, Japan objective). The recorded neurons were selected up to 50 μm below the slice surface. The fluorescent beads were identified using the same microscope with a filter cube for green fluorescent protein (Fig. 1*B*). Both fluorescence and IR-DIC images were taken by a camera (VX 55, Till Photonics, Gräfelfing, Germany) and displayed on a monitor (WV-BM 1410, Panasonic, Osaka, Japan). The cells identified under the fluorescence were marked on the monitor with the z coordinates given by the micromanipulators (SM-55, Luigs and Neumann, Ratingen, Germany) and could then be identified with certainty in the IR-DIC imaging for patch-clamp recordings (Fig. 1*D*).

Electrophysiological Recordings

Somatic whole-cell recordings were performed at 35 °C, and signals were amplified using Axoclamp-2B amplifiers (Axon Instruments, Molecular Devices, Union City, CA). Voltages were recorded with pipettes containing (in mM) 110 potassium gluconate, 10 KCl, 4 ATP-Mg, 10 phosphocreatine, 0.3 GTP, 10 *N*-2-hydroxyethylpiperazine-*N*′-2-ethanesulfonic acid (pH 7.3, 310 mOsm adjusted with sucrose), and 0.5% biocytin. The pipettes were pulled with a Flamming/Brown micropipette puller P-97 (Sutter Instruments Co, Novato, CA). The scaled output of the amplifier was connected to an ITC device (ITC-18, Instrutech Co, Port Washington, NY) connected to an Apple computer running Igor Pro (Wavemetrics, Portland, OR). The junction potential between the ACSF and the solution in the pipettes was around −10 mV. The recordings were made without correction for it.

Biocytin Labeling

The recording pipettes were filled with 5 mg mL^{-1} of biocytin that was perfused into the neurons during recording. Following the recording, the slices were fixed for at least 24 h in a cold phosphate buffer (100 mM, pH 7.4) containing 2% paraformaldehyde and 1% glutaraldehyde and 0.3% picric acid. Thereafter, the slices were rinsed and then transferred into a phosphate-buffered 3% H_2O_2 to block endogenous peroxidases. After rinsing in the phosphate buffer, slices were incubated overnight at 4 °C in an avidin-biotinylated horseradish peroxidase (ABC-Elite, Vector Labs, Burlingame, CA; 5% A, 5% B, and 0.25% Triton X-100). Subsequently, sections were rinsed again in the phosphate buffer and developed with diaminobenzidine (DAB substrate kit, Vector Labs) under visual control using a stereomicroscope (Leica, Wetzlar, Germany) until all processes of the cells were clearly visible. Finally, the reaction was stopped by transferring the sections into the phosphate buffer. After rinsing in the phosphate buffer, slices were mounted in an aqueous mounting medium.

Reconstruction

The stained cells were reconstructed under light microscope using Neurolucida software (MicroBrightField, Magdeburg, Germany). Reconstructed neurons and connections underwent quantitative analysis using NeuroExplorer (MicroBrightField). The quantitative morphometric analysis is based on multiple parameters derived from the dendrites and axons of reconstructed neurons. Putative contacts were identified according to the following criteria: (i) only the contacts formed by axonal swellings (boutons) were considered; (ii) the same plane of focus (microscope lens with 60× magnification, numerical aperture = 0.9; resolution along the z axis = 0.37 μm) is used. This requires the boutons and soma/dendrite/axon to be membranes within <0.5 μm of each other; (iii) if a dendrite is thick (>2 μm) with many spines, then a greater distance between the bouton and dendrite is allowed, providing that the course of the axon bent toward or ran parallel to the dendrite. When a putative contact was located, it was systematically double-checked through the eyepieces to confirm the screen-based identification. The staining procedure results in ~25% shrinkage of the slice thickness and ~10% anisotropic shrinkage along the x and y axes. Only the shrinkage of thickness was corrected.

Electrophysiological Analysis

The action potential (AP) onset is measured as the time point where the second derivative with respect to time of the voltage trace is maximum, that is, where the deflection of the curve is maximum. The end of the AP falling phase is measured as the time point where the modulus of the falling rate becomes lower than 5 V s^{-1}.

The excitatory postsynaptic potential (EPSP) onset was calculated by linear extrapolation from the 20–80% maximum amplitude linear fitting on the average trace of 80 single sweep events. These onset points were then automatically marked on the graph for visual verification. The latency of the single EPSP is defined as the time lapse between the top of the presynaptic AP and the EPSP onset. The coefficient of variation (CV) of the EPSP amplitude was calculated based on the measured amplitudes of each of the 80 single events triggered.

Model for Synaptic Dynamics

In order to analyze quantitatively the synaptic connections, a model of dynamic synaptic transmission was used (Markram et al. 1998). Fitting the responses to the model yielded 4 parameters: the time constant of recovery from depression, τ_D; the time constant of recovery from facilitation, τ_F; utilization of synaptic resources as used analogously to Pr (e.g., release probability), U; and the absolute strength, ASE, of the synaptic connection (defined as the response when Pr equals 1). After the 5th EPSP of a given train, the response typically reaches a steady-state amplitude considered to calculate the steady-state versus frequency (f) relationship. The frequency at which this curve matches a $1/f$ function is the limiting frequency. Tsodyks and Markram (1997) showed that if the presynaptic cell fires above the limiting frequency, the average postsynaptic depolarization will remain constant. The same study demonstrated that as lowering the calcium concentration increases the limiting frequency, this frequency is presynaptically dependent and estimated by $f \approx 1/(\tau_D \times Pr)$.

Results

Thirty-nine P11 Wistar rats were injected with fluorescent latex microbeads into layer V of the somatosensory cortex (S1). Rats appeared fully recovered within 2 days following the injection. The microbeads were clearly visible in acute slices under fluorescence microscopy, enabling selective recordings from neighboring (<100 μm somatic distance) CCPs (Fig. 1 *A,F*). A total of 476 marked cells were patched and filled with biocytin. The neuron somata were small and pyramidal shaped with a slender apical dendrite projecting toward the pia. Neurons with soma located in lower layer V had an apical dendrite projecting to layer II/III, whereas about 80% of the neurons located in more superficial layers had an apical dendrite reaching layer I (Fig. 1*E*). Labeled cells were visible in all the layers from layer II to layer VI in an area symmetrical to the injection site.

Single-Cell Electrophysiology

The response of CCPs to a step current injection was either an initial AP or a burst of 2–3 APs followed by a pause before firing again (Fig. 2*G*, defined as burst adapting) or an initial AP or burst followed by a regular spiking train (Fig. 2*H*). Both behaviors were observed at high and low current injections. Their small somata and dendrites are expected to yield a relatively high input resistance and indeed, the input resistance was 183 ± 67 MΩ (all values are given as mean ± standard deviation [SD], n = 22, Fig. 2*A,B*, Table 1), and the membrane time constant in response to a negative pulse (Δ pulse) was 20 ± 6 ms (Fig. 2*D*, Table 1). In response to a step current injection, CCPs displayed slow after-hyperpolarization (Fig. 2*C*) of 7.1 ± 3.2 mV. The spiking threshold was –32 ± 6 mV (Fig. 2*F*), and on about half of the cells, an initial burst was present (Fig. 2*F*). A typical AP had an amplitude of 60 ± 5 mV, a duration at half amplitude of 1.9 ± 0.3 ms, a rise time of 1.0 ± 0.2 ms, and a fall time of 3.2 ± 0.6 ms (Fig. 2*E*). Values for second APs in a train and other intrinsic parameters are given in Table 1.

CCP versus TTC Single-Cell Electrophysiology

In order to compare the single-cell electrophysiology of the CCPs with the TTCs, we recorded from 35 TTCs using the same protocol of Figure 2. The CCPs have an AP amplitude significantly smaller than the TTCs (60 ± 5 mV, n = 22 vs. 63 ± 5 mV, n = 35, respectively, mean ± SD). This difference is even larger in the second AP of a train generated by a depolarizing step current (45 ± 11 mV vs. 63 ± 6 mV). On the contrary, the AP duration is about 1.2 ms longer for the CCPs (4.3 ± 0.6 ms vs. 3.1 ± 0.5 ms for the first AP and 7.2 ± 1.2 ms vs. 6.0 ± 0.7 ms for the second AP in a train). The input resistance is 3.6 times larger in the CCPs (183 ± 67 MΩ vs. 51 ± 15 MΩ), but the membrane time

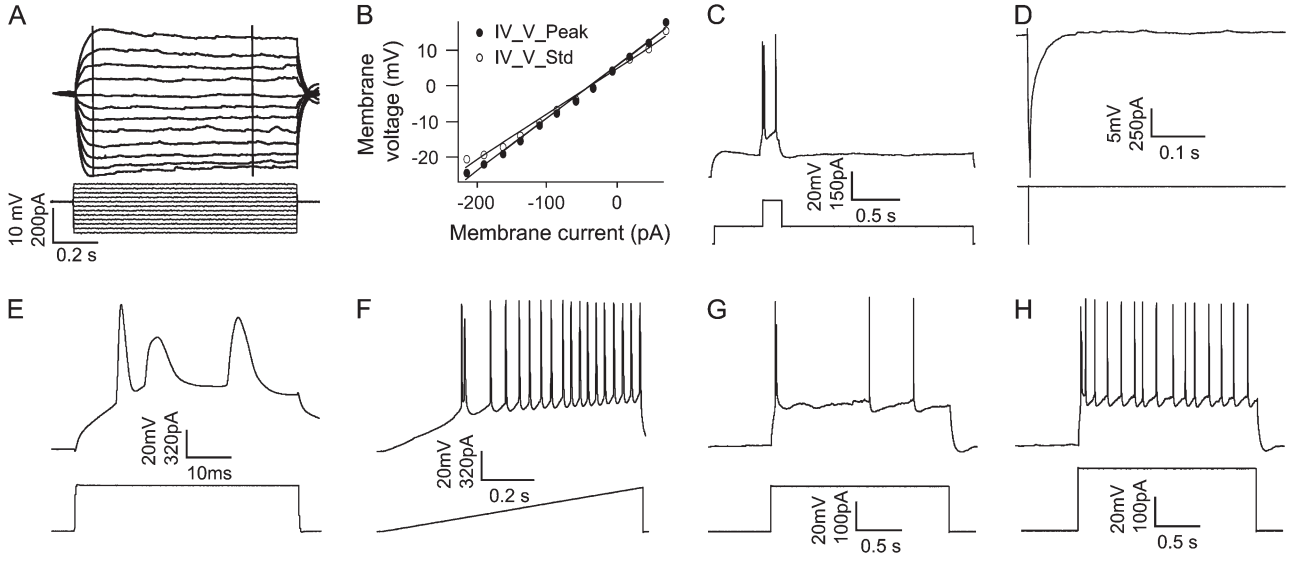

Figure 2. Single CCP electrophysiology. Recorded neurons are held at a membrane potential of −70 mV in current-clamp configuration. (*A*) Injected current steps and their corresponding voltage responses. (*B*) IV graph of the current–voltage relationship protocol described in (*A*). (*C*) Voltage response and current stimulation for slow after-hyperpolarization potential. (*D*) Voltage response and current stimulation of a short (5 ms) hyperpolarizing current injection used to determine the membrane time constant. (*E*) Voltage response and current stimulation of high temporal resolution used to determine the AP waveform. (*F*) Voltage response and current stimulation of a ramp to determine the discharge threshold. (*G*) Voltage response and current stimulation just above threshold to determine the threshold response to a long depolarizing pulse. (*H*) Same as in (*G*) but for more depolarized stimulation.

Table 1
Electrophysiological properties of the CCPs and the TTCs

	CCP (n = 22)	TTC (n = 35)
Access (MΩ)	23.7 ± 5.4	21.9 ± 4.9
First AP in train		
AP amplitude (mV)	59.6 ± 5.5	63.0 ± 5.3*
AP duration (ms)	4.29 ± 0.64	3.09 ± 0.52***
AP duration at half amplitude (ms)	1.93 ± 0.31	1.35 ± 0.24***
AP rise time (ms)	1.05 ± 0.16	0.80 ± 0.15***
AP fall time (ms)	3.24 ± 0.55	2.29 ± 0.41***
Fast AHP (mV)	−2.2 ± 4.1	3.7 ± 3.5***
Second AP in train		
AP amplitude (mV)	45 ± 11	63 ± 6***
AP duration (ms)	7.2 ± 1.2	6.0 ± 0.7***
AP duration at half amplitude (ms)	2.87 ± 0.88	2.06 ± 0.35***
AP rise time (ms)	1.99 ± 0.39	1.25 ± 0.26***
AP fall time (ms)	5.2 ± 1.1	4.7 ± 0.7
IV analysis		
Time to hyperpol peak (s)	0.194 ± 0.033	0.417 ± 0.430**
Input resistance for peak (MΩ)	228 ± 92	64 ± 19***
Input resistance for steady state (MΩ)	183 ± 67	51 ± 15***
Maximum sag (mV)	6.6 ± 3.9	5.8 ± 3.4
Decay time constant for Δ pulse (ms)	20.0 ± 5.8	17.5 ± 4.7
AP threshold (mV)	−32.3 ± 5.6	−39.4 ± 2.6***
Slow AHP (mV)	7.1 ± 3.2	8.6 ± 2.9
Step current		
Average delay to first spike (s)	0.031 ± 0.013	0.026 ± 0.012
Current-discharge slope (Hz nA^{-1})	27.6 ± 28.5	26.2 ± 5.7
Initial burst interval (s)	0.052 ± 0.047	0.081 ± 0.049*

Note: Mean ± SD, *$P < 0.05$, **$P < 0.01$, ***$P < 0.001$, P value is from Student t-test; AHP = after hyperpolarization.

constant after a hyperpolarizing spike is similar for both populations (20 ± 6 ms vs. 18 ± 5 ms). CCPs had a higher discharge threshold (-32 ± 6 mV vs -40 ± 3 mV), as extracted from a response to a ramp current injection (Fig. 2 F). Both populations have a similar mean current-discharge slope although its variation is much higher in the CCPs population than for the TTCs (28 ± 28 Hz nA^{-1} for CCPs and 26 ± 6 Hz nA^{-1} for TTCs). The initial burst interval is significantly smaller in the CCPs (50 ± 50 ms vs. 80 ± 50 ms) showing the tendency for some cells of this population to discharge with an initial burst in response to a depolarizing step current. The distribution of this interval for the CCPs is not showing 2 distinct groups indicating that the transition between bursting and not-bursting behavior is continuous in the CCPs population (bursting on Fig. 2*F* and not-bursting on Fig. 2*G*). None of the TTCs recorded showed this initial burst. The complete data set is given in Table 1.

Morphology of the Corticocallosal Cells

Consistent with previous reports (Katz 1987; Hubener and Bolz 1988; Christophe et al. 2005), the morphological differences of CCPs from TTCs were already obvious under light microscopy by the smaller soma and the untufted apical dendrites (Fig. 3*A*,*F*). These differences in the dendritic arborization are further quantified by the total dendritic tree surface (4800 ± 300 μm^2 for the CCPs vs. 33 000 ± 3000 μm^2 for TTCs) and by the dendritic Sholl distance (Fig. 3*B*), in which the number of intersections crossing concentric circles centered on the soma are counted (Fig. 3*A*). The Sholl analysis provides a quantitative estimate of the arborization of an axonal or dendritic tree. A greater number of crossings at a given distance compared with another indicate that it is more likely for the neuron to send outputs or receive inputs at that distance. The dendritic Sholl distance distribution of CCPs displayed a single peak within a radius of 100 μm from soma (Fig. 3*B*, red). The TTCs Sholl distance distribution shows clearly the tuft at a distance between 700 μm and 980 μm from the soma (Fig. 3*B*, gray). Moreover, the more extended dendritic tree of the TTCs is also visible on the Sholl distribution as the plot of Figure 3*B* is scaled by a factor of 0.51 for the TTCs. The axonal Sholl distance reflected the CCPs axons dense projection below the soma within a radius of 200 μm (Fig. 3*C*). Most of the cells had multiple primary axonal collaterals (collaterals directly emerged out from the main axonal stem, 7 ± 3). One of them often projected up ascending in parallel to the apical dendrite (70%, 15/22 reconstructed), with an averaged length of about 400 μm. Below the dense projection zone illustrated by the Sholl distance analysis, CCPs axons typically project 2 primary axonal collaterals horizontally extending within the layer VI (80%, 17/22 reconstructed, Fig. 3*A*). The main axonal trunk descends vertically into the white matter, presumably projecting to the opposite hemisphere. A summary of the morphological parameters is presented in Table 2.

Synaptic Connections between CCPs

In order to study the CCPs synaptic properties, we recorded simultaneously from labeled neurons with soma lying within a lateral distance of 100 μm. The probability to find a connection between 2 CCPs in acute slices was 3.15% (40 connections out of 1272 pairs tested). A single presynaptic AP induced an EPSP with amplitude of 0.8 ± 0.6 mV (Fig. 4*D*, mean ± SD). The latency (Fig. 4*C*), defined as the time lapse between the top of the AP and the EPSP onset, was 1.4 ± 0.8 ms (Fig. 4*D*). The 20–80% rise time was 2.8 ± 1.0 ms (Fig. 4*D*), and the decay time constant to rest membrane potential from the EPSP maximum amplitude (Tau) was 47 ± 25 ms (Fig. 4*D*). The mean number of synapses per connection obtained with the CV analysis was 4.6 ($n = [1–Pr_m]/[Pr_m \times CV_m^2]$, Pr_m: mean probability of release equivalent to U [see Materials and Methods], Fig. 6*D*, CV_m = mean CV, Fig. 5*C*). Morphological analysis yielded 4.0 ± 1.3 putative contacts per connection, in agreement with the CV analysis. Putative contacts between CCPs were mainly formed on basal dendrites (80%), at a branching order of 3.4 ± 0.2 (67.3% of total were formed on basal dendrites at a branching order higher than 3), a geometric distance of 129 ± 20 μm, and an electrotonic distance (see Materials and Methods) of 0.15 ± 0.02 (n = 14). The number of failures was relatively small and comparable to previously found values for other PC to PC connections (12 ± 11%, n = 23 [Thomson et al. 1993; Markram et al. 1997]). Despite this low failure rate, the observed CV was quite high (0.58 ± 0.24, n = 23). Weak synaptic connections displayed high trial-to-trial variability, as observed by the negative correlations between the mean EPSP size and the failure rate and CV (correlation index –0.73 and –0.74, respectively) and the positive correlations between the CV and failure rates (correlation index 0.92). These correlations show that the amplitudes of the CCPs to CCPs EPSPs depend on the number of synapses rather than on the probability of release. Among the correlations between the number of contact points, the distance of the contacts from the soma along the dendrites, the distance between the cell soma and the amplitude of the EPSP, only 3 were above 0.4. The correlation indices are 0.62 between the number of contact and the distance separating soma, 0.46 between the amplitude of the EPSP and the number of contact points, and 0.42 between the EPSP amplitude and the distance separating soma. It is worth to notice that given the small range of the data obtained for the soma separation distance (80 ± 40 μm, n = 14, mean ± SD) and the number of contact points

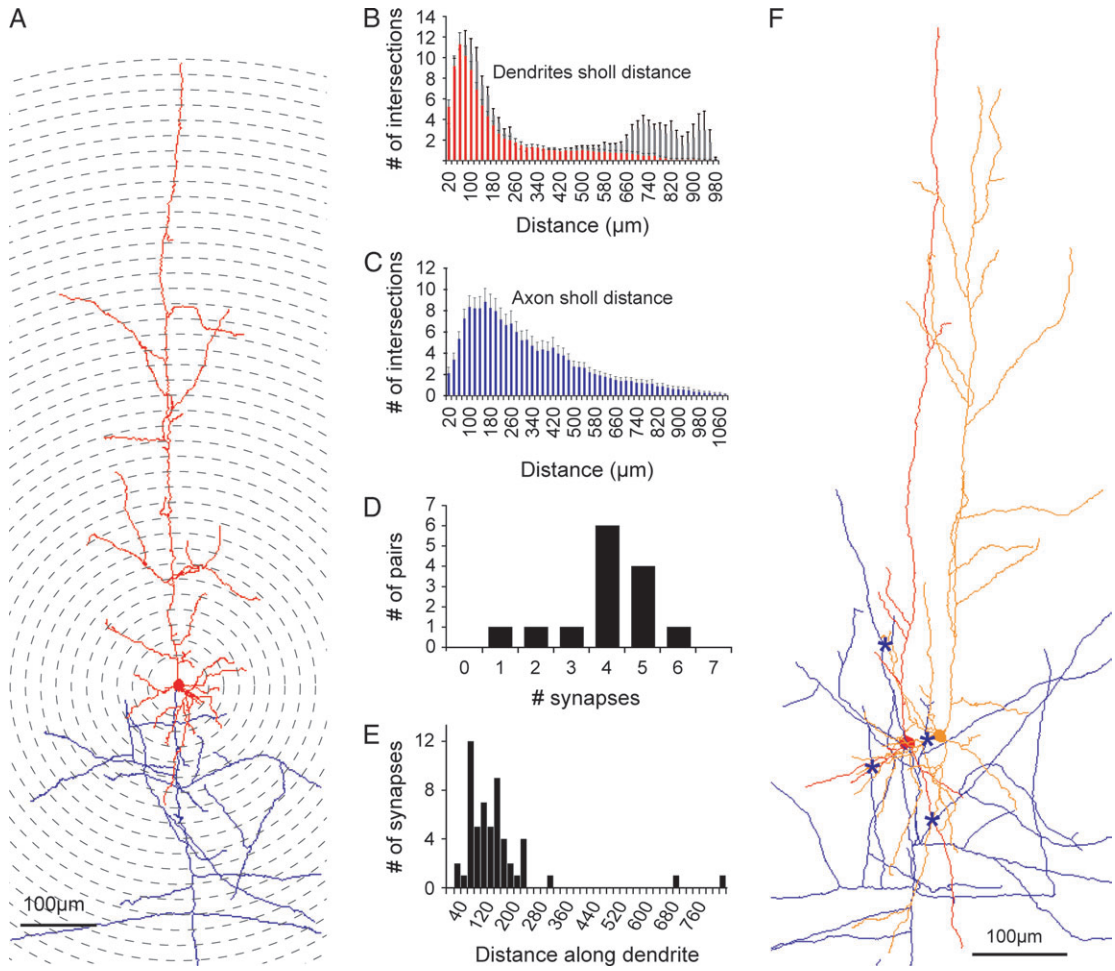

Figure 3. Morphological characteristics of single cell and connections in the CCP population. (*A*) Reconstruction of a single CCP showing the untufted apical dendrite and the circles defining the Sholl distances. Axon in blue and dendrites and soma in red. (*B*) Dendrite Sholl analysis. The distribution designates the number of times the circle centered on the soma with a radius of the Sholl distance crosses a dendrite (cf., *A*) ($n = 23$). Front in red: CCPs, behind in gray normalized with a factor of 0.51: TTCs (*C*) Axon Sholl analysis ($n = 23$), same as in (*B*). (*D*) Distribution of putative contacts in the population. A total of 4.0 ± 0.3 putative contacts per connection (mean ± SEM, $n = 14$). (*E*) Distribution of the distance between the soma and the putative contacts along the dendrites 130 ± 18 μm (mean ± SEM, $n = 55$). (*F*) Reconstruction of a pair of connected CCPs. Presynaptic axon in blue and dendrites in red and orange. Stars show the location of the identified putative contacts (axodendritic contact points with a bouton at the touch site).

Table 2
Morphometric properties of the corticocallosal PCs

	Mean	SEM	*n*
Dendritic tree surface (μm^2)	4800	300	23
Apical dendritic length (μm)	2973	1285	23
Basal dendrite number	5.2	1.5	23
Maximum branching order			
Apical dendrite	13.6	4.5	23
Basal dendrite	5.4	2	23
Axon	9.8	2.7	23

(Fig. 3*D*), more data would be required to reach any strong conclusion on this issue.

We used presynaptic trains of APs at various frequencies to characterize the dynamic properties of synaptic connections between CCPs (Figs 4*B* and 6). The synaptic responses were fitted using the model for synaptic dynamics, allowing for the extraction of the release probability and time constants of recovery from depression and facilitation (Markram et al. 1998) (see Materials and Methods and Fig. 6*B*). Synaptic connections between CCPs had low release probabilities (0.39 ± 0.14, range 0.04–0.61, $n = 23$, Fig. 6*D* top right panel), exhibited short-term depression (depression time constant: 690 ± 410 ms, Fig. 6*D* bottom left panel) and only little facilitation (facilitation time constant 44 ± 103 ms, Fig. 6*D* bottom right panel). We used presynaptic trains of different frequencies to extract the limiting frequency of CCP synapses (see Materials and Methods), which was found to be approximately 4 Hz (Fig. 6*C*).

CCP versus TTC Connectivity

We recorded from 24 synaptically connected TTCs pairs to perform a quantitative comparison with CCP pairs. TTCs were identified under IR-DIC microscopy by their large soma and thick apical dendrites. Neurons were biocytin filled via the patch pipette during recordings, and a later confirmation of the stained TTCs was obtained under light microscopy (as in Markram et al. 1997). The number of probed pairs was 222, giving 11% of connected pairs. This shows that the CCPs are 3–4 times less connected than the TTCs. A chi-square test yielded a P value of 8.10^{-17}. The EPSP amplitudes had a tendency to be smaller for the CCP synapses compared with TTC synapses (0.8 ± 0.2 mV for CCPs and 1.2 ± 0.2 mV for TTCs, mean ± standard error of the mean [SEM]).

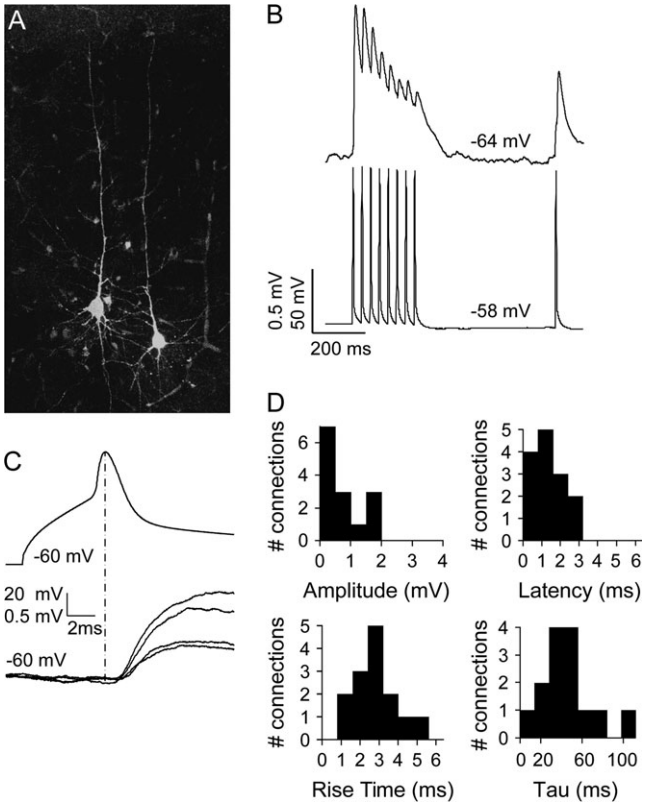

Figure 4. CCP connectivity: population response to a single AP. (*A*) Confocal image of a pair of layer V CCPs. (*B*) EPSP (top trace) recorded in response to the presynaptic cell stimulation of 8 APs at 30 Hz and a recovery test spike 500 ms later (bottom trace). Membrane potentials are given in the middle of the traces. (*C*) Single AP stimulated in the presynaptic cells (top trace) and 4 examples of trial-to-trial EPSP (bottom trace). The dashed line indicates the reference point for the latency measurement. Membrane potentials are given near the traces. (*D*) Population distribution of CCP single AP EPSP (80 trials per cell). Amplitude 0.8 ± 0.2 mV, latency 1.4 ± 0.2 ms, rise time 2.8 ± 0.3 ms, Tau = 47 ± 7 ms (membrane potential decay time constant from the top of the EPSP to rest) (mean ± SEM, n = 13 cells).

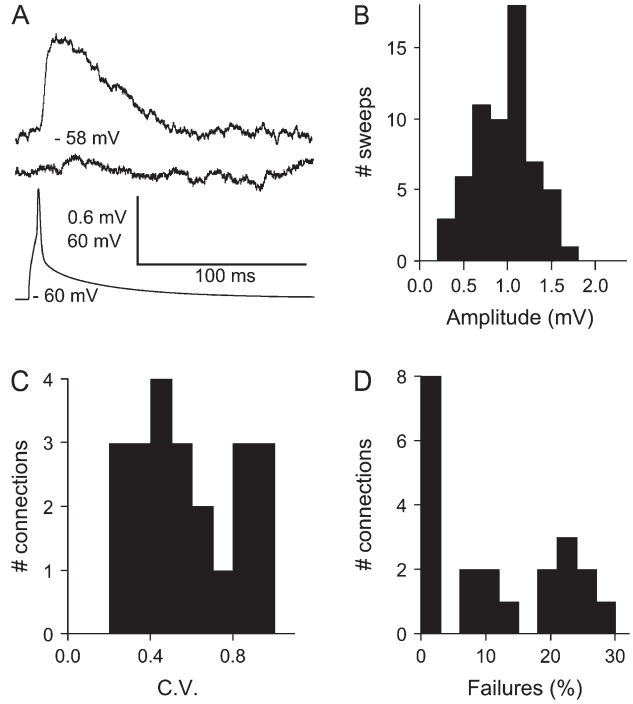

Figure 5. CCP connectivity: trial-to-trial response to a single AP. (*A*) Example of a successful EPSP, a failure and the corresponding presynaptic AP. Membrane potentials are given in the middle of the traces. (*B*) Distribution of the amplitudes for one cell across the trials (80 trials, 0.99 ± 0.06 mV, mean ± SEM). (*C*) Distribution of the CV for the CCP population (0.58 ± 0.05, n = 22). (*D*) Distribution of the failures for the CCP population (12 ± 2%, n = 22).

The onset latency for EPSPs was 1.4 ± 0.2 ms for CCPs and 1.2 ± 0.3 ms for TTCs; the 20–80% rise time was 2.8 ± 0.3 mV for the CCPs and 3.6 ± 0.6 ms for the TTCs; the synaptic decay time was 47 ± 7 ms for the CCPs and 54 ± 4 ms for the TTCs (mean ± SEM, n = 14 for CCPs and n = 12 for TTCs). None of these values was significantly different (P value larger than 0.2 in a 2-tailed t-test, data summarized in Table 3). Short-term plasticity was also compared between CCPs and TTCs (Fig. 7*A*,B) using the model for synaptic dynamics (see Materials and Methods). The only significantly different parameter was the probability of release (0.39 ± 0.03 vs. 0.51 ± 0.02 for CCPs and TTCs, respectively, mean ± SEM, P < 0.01 Fig. 7*C*, top panel). TTCs are interconnected by a disynaptic inhibitory pathway (Fig. 7*D*, first, second, and third panels) (Silberberg and Markram 2004; Rinaldi et al. 2005), which is activated following a presynaptic burst discharge. Such disynaptic inhibitory responses were not observed between CCPs, in contrast to their high prevalence between TTCs (Fig. 7*D*).

Discussion

Our study describes the properties of a subpopulation of neocortical pyramidal neurons projecting to the contralateral hemisphere. Whole-cell recordings from groups of layer V CCPs were obtained following retrograde labeling of the contralateral hemisphere and their morphological, electrophysiological, and synaptic properties were extracted. In agreement with previous reports (Katz 1987; Hubener and Bolz 1988; Mercer et al. 2005), CCPs had shorter and thinner apical dendrites, smaller soma, and higher input resistance than the thick tufted layer V PCs. In addition, the AP amplitude of the CCPs was smaller, and the AP duration was longer in the CCPs than in the TTCs. The discharge threshold was higher in the CCPs suggesting a lesser excitability of this PC type. We speculate that together with the AP duration, this lesser excitability could compensate for the higher input resistance and hence explain the similar current-discharge slope between the 2 populations.

Previous studies showed that some neurons in the guinea pig adult neocortex tend to discharge with an initial burst in response to a depolarizing step current (Connors et al. 1982). In a previous study, PCs that were morphologically undistinguishable exhibited discharge with or without an initial burst (McCormick et al. 1985). Another study reported that the large PCs (like the TTCs described here) displayed an initial burst discharge, whereas small PCs (closer to the CCPs) presented only a regular spiking behavior in the somatosensory cortex of 1-month-old rats (Chagnac-Amitai et al. 1990). Later, it was revealed that the bursting behavior of the TTCs originated from dendritic stimulations and regular firing originated from somatic stimulations (Schwindt and Crill 1999). Our results indicate that a variation of discharge behavior is true for the CCPs in the juvenile somatosensory neocortex. However, there are clear morphological and electrophysiological differences between the TTCs and the CCPs. Indeed, the main differences are in the shorter apical dendrite, larger input resistance, longer AP

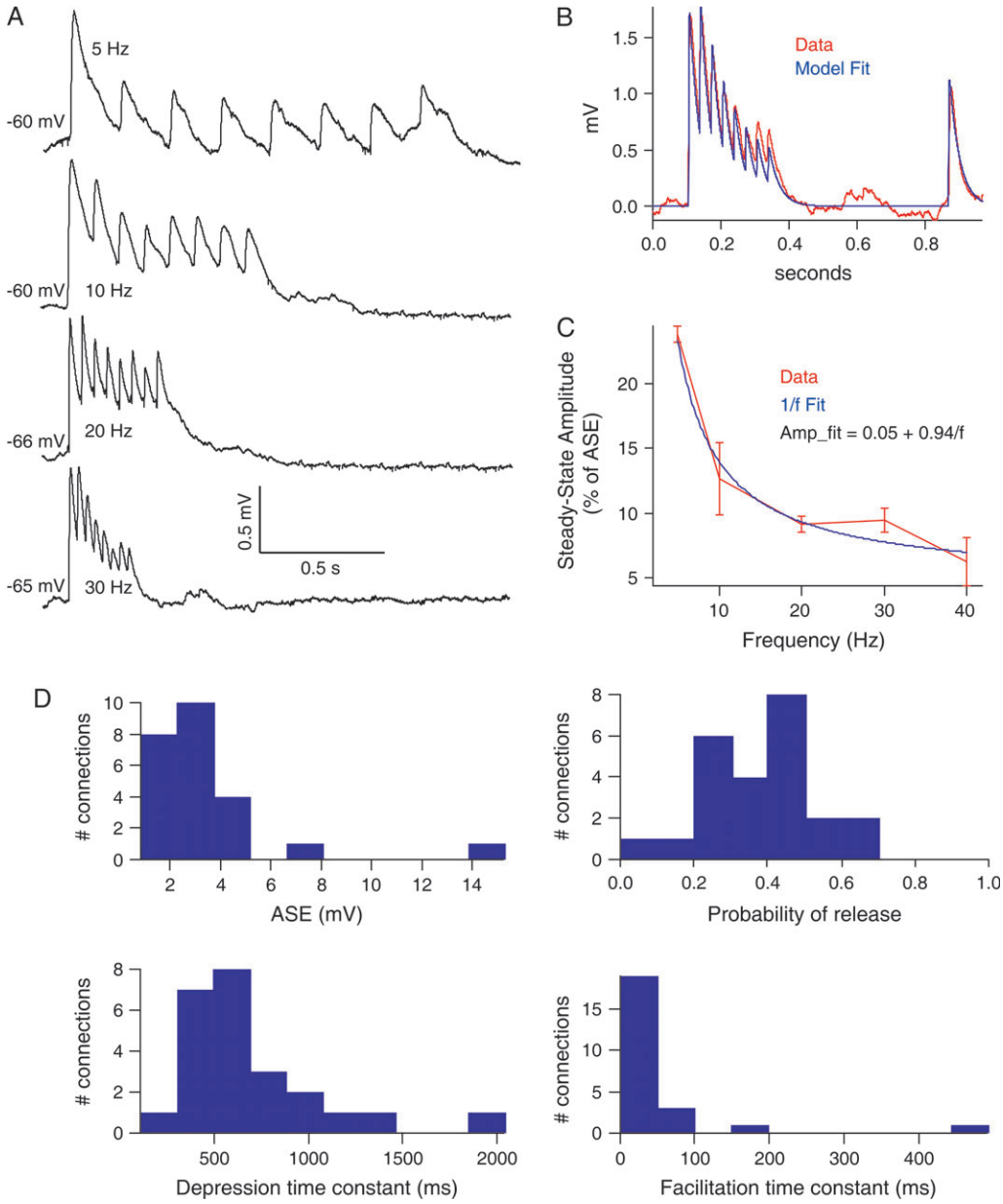

Figure 6. CCP connectivity: response to a train of APs. (*A*) Frequency dependence of EPSPs in response to a train of 8 APs at 5, 10, 20, and 30 Hz. Membrane potentials are given at the beginning of the traces. (*B*) Red trace: actual data for one connection averaged over 30 trials. Blue trace: Tsodyks–Markram model fit of the data. (*C*) Frequency dependence of the steady-state amplitude (last 3 EPSPs of the trains shown in panel *A* averaged and divided by the corresponding ASE). Blue trace: inverse frequency fit of the data trace, as given by the equation for Amp_fit. (*D*) Distributions of the parameters extracted by the Tsodyks–Markram model. ASE is the absolute synaptic efficacy, that is, the amplitude of the EPSP if the probability of release U was 1. ASE = 3.4 ± 0.6 mV, U = 0.39 ± 0.03, τ_D = 690 ± 90 ms, τ_F = 44 ± 21 ms (mean ± SEM, n = 23).

Table 3
Comparison of the synaptic properties between CCPs and TTCs

	CCP	TTC	*P* value
Number of putative contacts/connection	4.0 ± 0.3	5.5 ± 1.1[a]	<0.005
Amplitude (mV)	0.8 ± 0.2	1.2 ± 0.2	>0.02
Latency (ms)	1.4 ± 0.2	1.2 ± 0.3	>0.07
Rise time (20–80%, ms)	2.8 ± 0.3	3.6 ± 0.2	>0.02
Decay time (ms)	47 ± 7	54 ± 4	>0.03
ASE (mV)	3.4 ± 0.6	3.8 ± 0.4	>0.06
U	0.39 ± 0.03	0.51 ± 0.02	<0.01
τ_D (ms)	690 ± 90	620 ± 30	>0.03
τ_F (ms)	44 ± 21	13 ± 4	>0.01

Note: Student *t*-test was used for the statistical comparison.
[a]Data obtained from Markram et al. (1997).

duration, smaller AP amplitude, and the presence of an initial burst for the CCPs compared with the TTCs. The mechanism underlying bursting was suggested to be dependent on the synchronicity of the sodium spike with a dendrite generated calcium spike (Schwindt and Crill 1999). The bursting behavior of some CCPs reported here might depend on various intrinsic properties that are related to the dendritic calcium spike. Intrinsic neuronal properties depend on the developmental stage of the tested animals, which may also be a reason for the variability in firing patterns recorded in different studies.

Synaptic connections between pairs of CCPs were characterized and compared with those observed between TTCs. Synaptic connections between CCPs differed in their low

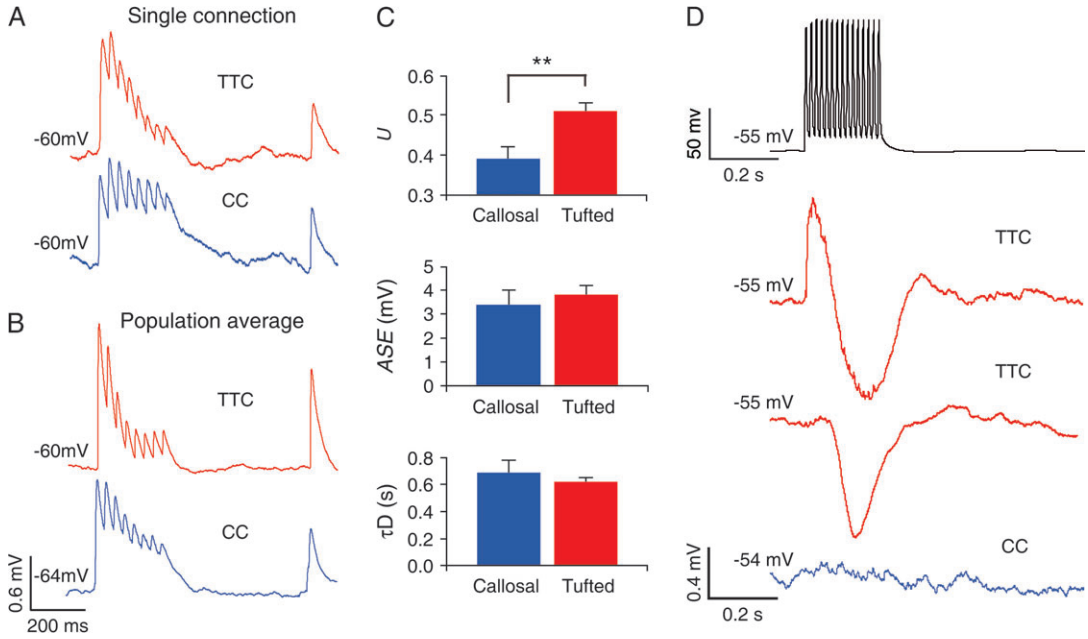

Figure 7. Comparison of CCP connection dynamics with the TTC. (*A*) Comparison of an EPSP response to an 8 APs train at 30 Hz followed by a recovery test AP 500 ms later. Red trace: TTC single connection and blue trace: CCP single connection. Membrane potentials are given at the beginning of the traces. (*B*) Same as (*A*) but traces are population averages ($n = 13$ for CCPs and $n = 10$ for TTCs). (*C*) Parameters extracted by the Tsodyks–Markram model. $^{**}P < 0.01$, CCP $n = 23$, TTC $n = 24$ (CCP: $U = 0.39 \pm 0.03$, ASE = 3.4 ± 0.6 mV, $\tau_D = 690 \pm 90$ ms; TTC: $U = 0.51 \pm 0.02$, ASE = 3.8 ± 0.4 mV, $\tau_D = 620 \pm 30$ ms, mean ± SEM). (*D*) Disynaptic connection between PCs mediated by an interneuron. First panel shows a presynaptic stimulation used to evoke the disynaptic connection (15 APs at 70 Hz). Second and third panels show a TTC disynaptic inhibitory response with and without a direct monosynaptic connection, respectively. Fourth panel shows a CCP response, whereas another CCP was stimulated at 70 Hz. No disynaptic connections were observed between CCPs. Membrane potentials are given at the beginning of the traces.

connection probability, smaller EPSP amplitudes, and lower release probabilities. Disynaptic inhibition was not observed between CCPs pairs, compared with the large probability for these connections between TTCs. Our results show that in addition to differences in the morphological and electrophysiological properties, subpopulations of PCs within the same neocortical column and layer also display different properties of connectivity.

The short untufted apical dendrites of CCPs as well as the narrow span of their basal dendrites suggest that, unlike TTCs, they integrate inputs in a relatively narrow range. This is further supported by the almost complete absence of dendritic arborization in layers II/III, in which long-range horizontal intracortical connections are abundant (Fitzpatrick 1996; Chisum and Fitzpatrick 2004). CCPs do not display a dendritic tuft in layer I, suggesting that they also do not receive top–down inputs (Rockland and Virga 1989; Cauller and Connors 1994; Cauller et al. 1998). The untufted aspect of the CCPs apical dendrite is not a developmental feature due to incomplete dendritic growth because the dendritic arborization is already completed by the end of the first postnatal week (Wise and Jones 1976). Further, untufted morphology also exist in adult animals (Kasper et al. 1994). Putative contacts between CCPs were mainly located on basal dendrites, similar to those formed between TTCs, but different from those formed between corticostriatal PCs (Morishima and Kawaguchi 2006). Comparing with the TTC connections (5.5 ± 1.1, $n = 19$) (Markram et al. 1997), the CCPs formed a significantly smaller number of putative contacts in a connection (4.0 ± 0. 3, $n = 14$; $P < 0.005$, Student *t*-test). Connections between TTCs had 63% of contacts located on basal dendrites, and 37.5% of all contacts were formed on basal dendrite at an order higher than 3 (Markram et al. 1997) innervating to a greater extent the apical dendrite than the CCPs (80% of contacts on basal dendrites and 67.3% of contacts were on basal dendrites at a branching order higher than 3). The mean geometrical distance between the soma and the contact points tends to be larger in TTCs (201 ± 62 μm compared with 129 ± 20 μm for CCPs); however, the mean electrotonic distance is similar for both cell types as TTCs contacts are located at a mean electrotonic distance of 0.13 ± 0.03 (Markram et al. 1997) (0.15 ± 0.02 for CCPs).

The connection probability between CCPs was much lower than observed between TTCs, indicating different connectivity patterns for PCs in somatosensory cortex projecting to different targets. Similar differences in connectivity probabilities were observed between PCs in the prefrontal cortex projecting to different targets (Morishima and Kawaguchi 2006). The sparse connectivity between CCPs suggests that they may primarily be driven by other sources of excitation such as PCs from other subpopulations within layer V or from other layers. The connectivity between CCPs and other subclasses of PCs is, however, yet to be investigated. Given the differences reported here between the CCPs and TTCs circuits, it is very likely that there is an asymmetry in the connections between the PCs subpopulations (Thomson and Bannister 2003). The inhibitory network signaling to CCPs should also be considered in face of the specific excitatory connectivity pattern. Previous studies showed that Martinotti cells provide inhibition primarily to layers I and IV (Wang et al. 2004). These interneurons also mediate a disynaptic feedback loop within the TTCs population (Silberberg and Markram 2004). We did not observe any disynaptic inhibitory responses between CCPs, suggesting that the inhibitory connectivity also differs for various PC subpopulations.

This hypothesis is supported by a morphological study of the inhibitory synapses onto the TTCs and CCPs populations (Farinas and DeFelipe 1991) in the cat visual cortex that shows a higher axosomatic inhibitory synapses density on the CCPs. This population would then be less innervated distally and more somatically than the TTCs. The differential distribution of inhibitory synapses between cell populations projecting to different target has also been shown in the monkey (Lund et al. 2001), indicating that this projection target specificity for inhibition might not be specific to species.

Most synaptic properties, such as onset latency, kinetics, depression, facilitation, were similar for connections between CCPs and between TTCs. However, connections between CCPs were weaker and had lower release probabilities, following the same tendency of very low interconnectivity in this subpopulation.

This low interconnectivity suggests a reduced integration capacity of the CCP population as compared with the thick tufted pyramidal network. The rather linear dynamics of the connections between CCPs also suggests a different functional role in the neocortex compared with the TTCs. The narrower dendritic field of the CCPs further indicates that this population mainly receives and processes information present in the microcolumn and the neighboring layers, thus integrating inputs from a smaller area than the TTCs. We therefore speculate that CCPs contribute less to the processing within the column than TTCs and perform minimal transformation of the information processed before sending it to the opposite hemisphere. The CCP cells therefore appear to be well suited to act as read out neurons of the columns for the opposite hemisphere.

Notes

Conflict of Interest: None declared.

Address correspondence to email: henry.markram@epfl.ch

References

Aboitiz F, Lopez J, Montiel J. 2003. Long distance communication in the human brain: timing constraints for inter-hemispheric synchrony and the origin of brain lateralization. Biol Res. 36:89–99.

Cauller LJ, Clancy B, Connors BW. 1998. Backward cortical projections to primary somatosensory cortex in rats extend long horizontal axons in layer I. J Comp Neurol. 390:297–310.

Cauller LJ, Connors BW. 1994. Synaptic physiology of horizontal afferents to layer I in slices of rat SI neocortex. J Neurosci. 14: 751–762.

Chagnac-Amitai Y, Luhmann HJ, Prince DA. 1990. Burst generating and regular spiking layer 5 pyramidal neurons of rat neocortex have different morphological features. J Comp Neurol. 296:598–613.

Chisum HJ, Fitzpatrick D. 2004. The contribution of vertical and horizontal connections to the receptive field center and surround in V1. Neural Netw. 17:681–693.

Cho RH, Segawa S, Okamoto K, Mizuno A, Kaneko T. 2004. Intracellularly labeled pyramidal neurons in the cortical areas projecting to the spinal cord. II. Intra- and juxta-columnar projection of pyramidal neurons to corticospinal neurons. Neurosci Res. 50:395–410.

Christophe E, Doerflinger N, Lavery DJ, Molnar Z, Charpak S, Audinat E. 2005. Two populations of layer v pyramidal cells of the mouse neocortex: development and sensitivity to anesthetics. J Neurophysiol. 94:3357–3367.

Connors BW, Gutnick MJ, Prince DA. 1982. Electrophysiological properties of neocortical neurons in vitro. J Neurophysiol. 48: 1302–1320.

Eliassen JC, Baynes K, Gazzaniga MS. 2000. Anterior and posterior callosal contributions to simultaneous bimanual movements of the hands and fingers. Brain. 123(Pt 12):2501–2511.

Engel AK, Konig P, Kreiter AK, Singer W. 1991. Interhemispheric synchronization of oscillatory neuronal responses in cat visual cortex. Science. 252:1177–1179.

Farinas I, DeFelipe J. 1991. Patterns of synaptic input on corticocortical and corticothalamic cells in the cat visual cortex. I. The cell body. J Comp Neurol. 304:53–69.

Fitzpatrick D. 1996. The functional organization of local circuits in visual cortex: insights from the study of tree shrew striate cortex. Cereb Cortex. 6:329–341.

Hirsch JA, Gallagher CA, Alonso J-M, Martinez LM. 1998. Ascending projections of simple and complex cells in layer 6 of the cat striate cortex. J Neurosci. 18:8086–8094.

Hubener M, Bolz J. 1988. Morphology of identified projection neurons in layer 5 of rat visual cortex. Neurosci Lett. 94:76–81.

Kasper EM, Larkman AU, Lubke J, Blakemore C. 1994. Pyramidal neurons in layer 5 of the rat visual cortex. I. Correlation among cell morphology, intrinsic electrophysiological properties, and axon targets. J Comp Neurol. 339:459–474.

Katz LC. 1987. Local circuitry of identified projection neurons in cat visual cortex brain slices. J Neurosci. 7:1223–1249.

Lund JS, Griffiths S, Rumberger A, Levitt JB. 2001. Inhibitory synapse cover on the somata of excitatory neurons in macaque monkey visual cortex. Cereb Cortex. 11:783–795.

Markram H, Lubke J, Frotscher M, Roth A, Sakmann B. 1997. Physiology and anatomy of synaptic connections between thick tufted pyramidal neurones in the developing rat neocortex. J Physiol. 500(Pt 2):409–440.

Markram H, Wang Y, Tsodyks M. 1998. Differential signaling via the same axon of neocortical pyramidal neurons. Proc Natl Acad Sci USA. 95:5323–5328.

Matsuzaka T, Ono K, Baba H, Matsuo M, Tanaka S, Kamimura N, Tsuji Y. 1999. Quantitative EEG analyses and surgical outcome after corpus callosotomy. Epilepsia. 40:1269–1278.

McCormick DA, Connors BW, Lighthall JW, Prince DA. 1985. Comparative electrophysiology of pyramidal and sparsely spiny stellate neurons of the neocortex. J Neurophysiol. 54:782–806.

Mercer A, West DC, Morris OT, Kirchhecker S, Kerkhoff JE, Thomson AM. 2005. Excitatory connections made by presynaptic corticocortical pyramidal cells in layer 6 of the neocortex. Cereb Cortex. 15:1485–1496.

Morishima M, Kawaguchi Y. 2006. Recurrent connection patterns of corticostriatal pyramidal cells in frontal cortex. J Neurosci. 26:4394–4405.

Quigley M, Cordes D, Turski P, Moritz C, Haughton V, Seth R, Meyerand ME. 2003. Role of the corpus callosum in functional connectivity. Am J Neuroradiol. 24:208–212.

Rinaldi T, Silberberg G, Markram H. 2005. Enhanced monosynaptic and disynaptic connectivity in the neonatal microcircuit of an animal model of Autism. Abstract viewer/Itinerary Planner. Washington (DC): Society for Neuroscience Poster No. 448.2.

Rockland KS, Virga A. 1989. Terminal arbors of individual "feedback" axons projecting from area V2 to V1 in the macaque monkey: a study using immunohistochemistry of anterogradely transported Phaseolus vulgaris-leucoagglutinin. J Comp Neurol. 285:54–72.

Schwindt P, Crill W. 1999. Mechanisms underlying burst and regular spiking evoked by dendritic depolarization in layer 5 cortical pyramidal neurons. J Neurophysiol. 81:1341–1354.

Silberberg G, Markram H. 2004. Di-synaptic inhibition between pyramidal neurons via Martinotti cells in neocortical layer V. Abstract viewer/Itinerary Planner. Washington (DC): Society for Neuroscience Poster No. 508.7.

Simons DJ, Woolsey TA. 1984. Morphology of Golgi-Cox-impregnated barrel neurons in rat SmI cortex. J Comp Neurol. 230:119–132.

Thomson AM, Bannister AP. 2003. Interlaminar connections in the neocortex. Cereb Cortex. 13:5–14.

Thomson AM, Deuchars J, West DC. 1993. Large, deep layer pyramid-pyramid single axon EPSPs in slices of rat motor cortex display paired pulse and frequency-dependent depression, mediated presynaptically

and self-facilitation, mediated postsynaptically. J Neurophysiol. 70:2354–2369.
Tsiola A, Hamzei-Sichani F, Peterlin Z, Yuste R. 2003. Quantitative morphologic classification of layer 5 neurons from mouse primary visual cortex. J Comp Neurol. 461:415–428.
Tsodyks MV, Markram H. 1997. The neural code between neocortical pyramidal neurons depends on neurotransmitter release probability. Proc Natl Acad Sci USA. 94:719–723.
Vercelli AE, Garbossa D, Curtetti R, Innocenti GM. 2004. Somatodendritic minicolumns of output neurons in the rat visual cortex. Eur J Neurosci. 20:495–502.
Wang Y, Toledo-Rodriguez M, Gupta A, Wu C, Silberberg G, Luo J, Markram H. 2004. Anatomical, physiological and molecular properties of Martinotti cells in the somatosensory cortex of the juvenile rat. J Physiol. 561:65–90.
White EL, Hersch SM. 1982. A quantitative study of thalamocortical and other synapses involving the apical dendrites of corticothalamic projection cells in mouse SmI cortex. J Neurocytol. 11: 137–157.
Wise SP, Jones EG. 1976. The organization and postnatal development of the commissural projection of the rat somatic sensory cortex. J Comp Neurol. 168:313–343.
Yuste R. 2005. Origin and classification of neocortical interneurons. Neuron. 48:524–527.
Zhang ZW, Deschenes M. 1997. Intracortical axonal projections of lamina VI cells of the primary somatosensory cortex in the rat: a single-cell labeling study. J Neurosci. 17:6365–6379.
Zhang ZW, Deschenes M. 1998. Projections to layer VI of the posteromedial barrel field in the rat: a reappraisal of the role of corticothalamic pathways. Cereb Cortex. 8:428–436.